EI SEVIER

Contents lists available at ScienceDirect

Chemical Physics Letters

journal homepage: www.elsevier.com/locate/cplett



Research paper

Comparing the collision-induced dissociation of trimethyl lysine⁺ and acetyl lysine-H⁺



George L. Barnes a,*, Kristopher J. Kolonko b, Kenneth Lucas c,1, Amy Chen c,2, Megan Schubmehl c

- ^a Department of Chemistry, Illinois State University, Campus Box 4160, Normal, IL 61790-4160, United States of America
- b Stewart's Advanced Instrumentation and Technology (SAInT) Center, Siena College, 515 Loudon Road, Loudonville, NY 12211, United States of America
- ^c Department of Chemistry and Biochemistry, Siena College, 515 Loudon Road, Loudonville, NY 12211, United States of America

HIGHLIGHTS

- TMe-lysine⁺ and acetyl-lysine-H⁺ have nearly identical m/z ratios.
- Acetyl-lysine-H⁺ exhibits initial N-/Cterminus collision-induced dissociation.
- Acetyl-lysine-H⁺ show higher decomposition rates than TMe-lysine⁺.

GRAPHICAL ABSTRACT

Initial CID Loss Pathway

OH O=C
$$H_2$$
 H_2 H_2 H_2 H_2 H_3 H_4 H_5 H_5

ARTICLE INFO

Keywords: Collision-induced dissociation Post-translational modification Direct dynamics simulation Graph theory

ABSTRACT

Experimental and computational results are reported on the reaction dynamics taking place within the collision-induced dissociation (CID) of N_{ε} , N_{ε} , N_{ε} -Trimethyl-L-lysine⁺ (TMe-lysine⁺) and N_{ε} -acetyl-L-lysine-H⁺ (acetyl-lysine-H⁺). These common post-translational modifications result in a mass difference of only 0.036 Dalton. Resolving these two species directly requires a high-resolution instrument and they share several CID peaks. Nevertheless, the mechanisms observed are strikingly different, particularly at lower internal energies. Reactivity is higher for acetyl-lysine-H⁺, with decomposition initiated via losses at the N- and C-termini. In contrast, unmodified lysine and TMe-lysine⁺ exhibit mechanisms that involve an initial loss from the sidechain.

1. Introduction

Post-translational modifications (PTMs) of amino acids are common and result in an expanded functionality of proteins [1–3]. Methylation and acetylation of lysine are frequently observed within histone proteins. Tri-methylation and acetylation of a lysine at the side chain results in an mass difference of only ~ 0.036 Da, which requires high-resolution mass spectrometers to distinguish. However, the nature of these two species is considerably different. Tri-methylation of lysine by its very nature results in a charged species, while acetylation of the lysine side-chain results in no charge present. This fundamental difference results in significant changes in the reaction dynamics that take place during collision-induced dissociation (CID). The study of

PTMs via tandem mass spectrometry (MS2) and CID is a common task both experimentally [4–7] and computationally [8–13]. In our prior work, we examined mono-, di, and tri-methylation of lysine using both techniques [14]. In this work, we will directly examine the differences between $N_{\varepsilon},~N_{\varepsilon},~N_{\varepsilon}$ -Trimethyl-L-lysine (TMe-lysine+) and N_{ε} -acetyl-L-lysine-H+ (acetyl-lysine-H+) using experimental and computational means. Computationally, we employ direct dynamics simulations [11,12] to sample the chemical reactivity of both TMe-lysine+ and acetyl-lysine-H+, and reveal atomic level information regarding the mechanisms of CID in each system. As in our previous study, we will analyze the direct dynamics simulations by employing graph theory, which has recently become a popular means of gaining deeper insight into such results [9,10,14–19]. The use of graph theory

E-mail address: gbarnes@siena.edu (G.L. Barnes).

^{*} Corresponding author.

Presently at SUNY Upstate Medical University; College of Medicine;766 Irving Avenue; Syracuse, NY 13210.

 $^{^2\,}$ ACS Project SEED High School Student; Presently pursing an undergraduate degree at Northwestern University.

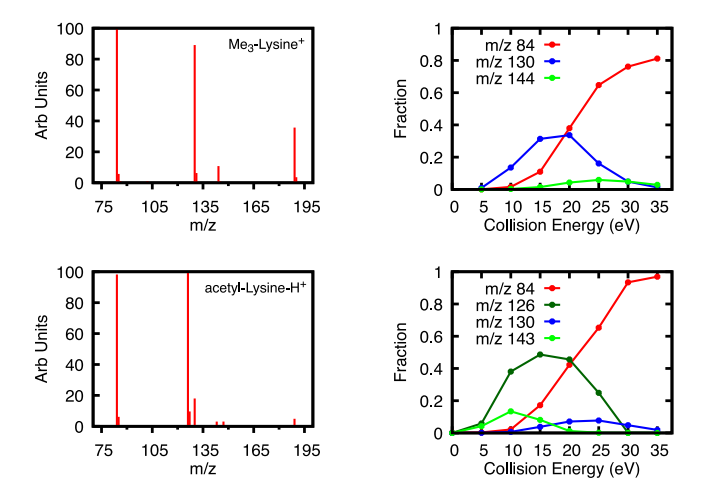


Fig. 1. The experimental MS2 spectra for TMe-lysine⁺ and acetyl-lysine-H⁺ for a collision energy of 20 eV in the first column with experimental break-down curves provided in column 2. In the first column, the spectrum intensity is scaled to the most intense peak for each given spectrum. In the second column, the experimental break-down curves are relative to the total ion signal collected. The greater diversity in MS2 decomposition peaks for acetyl-lysine-H⁺ is apparent.

allows for a straight-forward analysis of the isomers present for a given peak in a theoretical mass spectrum, as was illustrated in our previous work on methylated lysine [14].

An outline for the remainder of the paper is as follows: in Section 2, we provide an overview of our computational and experimental methods; in Section 3, we present our results and compare the CID pathways between TMe-lysine $^+$ and acetyl-lysine- H^+ ; and in Section 4, we provide a summary.

2. Methods

2.1. Computational approach

The techniques to simulate CID of MS2 systems are well documented in the literature [8,11,20]. Moreover, this work uses the results for TMe-lysine⁺ that were initially calculated by some of us in Lucas et al. [14] along with new simulations for acetyl-lysine-H⁺. Although no new TMe-lysine⁺ trajectory calculations were performed in this work, we will discuss the general method employed in our prior work. Below, we will briefly describe the approach and refer the interested reader to the literature for greater details.

2.1.1. Structures and simulation method

Initial structures for both TMe-lysine⁺ and acetyl-lysine-H⁺ were generated using Avogadro [21]. TMe-lysine⁺ naturally has a +1 charge located at the side-chain PTM, while an excess proton was placed on the N-terminus of acetyl-lysine-H⁺. A simulated anneal approach using GROAMCS [22] and the Gromas 54A7 [23] potential modified using the Automatic Topology Builder [24–26] was implemented to obtain candidate low-energy structures through six heat-cool cycles in which the temperature was ramped to 1000 K over 100 ps, held at 1000 K for 100 ps and then cooled to 0 K over 100 ps. The resulting 0 K structures were optimized at the RM1 semi-empirical method [27] level as implemented in Mopac2016 [28]. RM1 has produced good results for many previous MS2 simulations of protonated peptides [13,14,20,29–31]. The structure with the lowest energy for each TMe-lysine⁺ and acetyl-lysine-H⁺ were selected as the starting point for our direct dynamics simulations.

In our previous work involving TMe-lysine⁺ [14], we used a microcanonical sampling scheme to impart a statistical distribution of internal energy [32], which produced results that are in good agreement

with experiment. In that work, the most reactivity occurred for TMelysine⁺ with an internal energy of 400 kcal/mol; however, trajectories are also available with internal energies of 300, 350 kcal/mol. In this work, we will use the 300 and 400 kcal/mol trajectories as our initial data set for TMe-lysine+. For acetyl-lysine-H+, we ran test trajectories for a range of internal energies and determined that sufficient reactivity was observed at 300 kcal/mol. As described in the results and discussion section, pseudo MS3 simulations were performed with an internal energy of 250 kcal/mol starting from a acetyl-lysine-H+decomposition product to sample rare events. For each internal energy considered, 400 trajectories were calculated. The selected range of internal energies allowed for sufficient reactivity to explore the chemical space without producing large populations of low-mass products. Trajectories were numerically integrated using Hamilton's equation of motion along with a 6th order symplectic integration scheme [33], for a maximum simulation time of 50 ps with a 1 fs step size and output written every 50 fs using our in-house simulation package tightly coupled with Mopac2012 [34]. Given our focus is on charged fragments, neutral fragments were removed from the simulation when they were at least 15 Å away from a charge center. Trajectories were halted if the final charged fragment had an $m/z \le 60$. All trajectories had excellent conservation of energy.

Simulated mass spectra were obtained using the same methods our group has described previously [9,35]. Briefly, our in-house simulation code calculates and reports a connectivity matrix every 50 fs based on a bond order matrix that is averaged over a 5 fs window. In post analysis, these matrices are used to determine when connectivity changes, such as fragmentation events and proton transfers. Combining this information with a graph theory analysis [17,18] of final products allows for the automatic determination of structures associated with a particular m/z peak.

2.2. Experimental approach

High purity samples of N_{ε} , N_{ε} , N_{ε} -Trimethyl-L-lysine and N_{ε} -acetyl-L-lysine, acetonitrile were obtained from Sigma Aldrich and used without further purification. All samples were prepared in a mass spectrometry grade 1:1 mixture of acetonitrile and water. High-resolution mass spectrometry data was acquired on a Bruker Maxis Impact HD (Quadrupole-Time of Flight) spectrometer using sodium formate solution as the mass calibrant and the standard heated electrospray ionization (ESI) source. Pseudo MS3 experiments were performed utilizing in-source fragmentation. Typical collision energies considered were 5, 10, 15, 20, 25, 30, and 35 eV using nitrogen within the CID cell.

3. Results and discussion

3.1. Overview and general comparison between acetyl-lysine- H^+ and TMelysine+

While the nominal mass of both acetyl-lysine-H⁺ and TMe-lysine⁺ are identical and the experimental measurements show that the two systems share several decomposition peaks, their reactivity is strikingly different. An overview of the experimental results is provided in Fig. 1 which shows an example MS2 spectra at a collision energy of 20 eV along with the experimental break-down curves. One immediate observation apparent from the experimental data regarding the amount of parent ion remaining is that acetyl-lysine-H⁺ is significantly more reactive than TMe-lysine⁺. This is also seen in the direct dynamics simulations. Again, It should be noted that TMe-lysine⁺ has no excess proton and that the charge arises from the nature of the side-chain modification. This lack of an excess proton is likely the primary reason for its reduced reactivity. While at lower collision energies, there are significant differences in the experimental results, it is seen that at large collision energies, both species result in the *m/z* 84 peak preferentially.

Table 1 A comparison of the major peaks observed in the simulated mass spectrum of acetyllysine- H^+ at 300 kcal/mol and TMe-lysine+ at 300 and 400 kcal/mol reported as a fraction of all calculated trajectories. Products that result from the pseudo MS3 calculations starting from the m/z 143 decomposition product of acetyl-lysine- H^+ at 250 kcal/mol are also shown.

m/z	acetyl-lysine-H ⁺ 300 kcal/mol	m/z 143 ^a 250 kcal/mol	TMe-lysine ⁺ 300 kcal/mol	TMe-lysine ⁺ 400 kcal/mol
84 ^{b,c}	0.005*	0.036*	0.01*	0.22*
130^{b}	0.01*	0*	0.01*	0.103*
101 ^c	0	0.052	0	0
126 ^c	0*	0.019*	0	0
143 ^c	0.315*	0.852*,d	0	0.015
189 ^d	0.611	NA	0.968	0.483

- * Significant experimental product.
- $^{\rm a}$ Pseudo MS3 starting from primary m/z 143 structure seen in acetyl-lysine-H+.
- b Loss includes a portion of the side-chain.
- c Loss of either C(OH), or H2O + CO.
- ^d No fragmentation occurred.

Our simulations provided additional information, and we start our computational analysis by comparing the relative intensity of the most common peaks observed in our simulations for each system in Table 1. While acetyl-lysine-H $^+$ is more reactive, it is noteworthy that most of that reactivity occurs away from the PTM and involves the N- and G- termini. This is a striking observation as most of the reactivity in TMe-lysine $^+$ is initiated at the side-chain. Hence, it can be concluded that the acetylation has hindered reactivity at the side chain in contrast to trimethylation, which retains more reactivity, primarily through the formation of trimethyl amine. While m/z 126 is a common experimental peak, it is not commonly seen in simulations, which will be discussed more below.

3.2. Reactive pathways for acetyl-lysine-H⁺

Our experimental measurements find that at moderate collision energies the primary CID product of acetyl-lysine-H⁺ (m/z 189 – $[\mathrm{H}_{17}\mathrm{C_8}\mathrm{N_2}\mathrm{O_3}]^+$) is m/z 126 – $[\mathrm{H}_{12}\mathrm{C_7}\mathrm{NO}]^+$, which corresponds to the loss of $\mathrm{H_2}\mathrm{O}$ + CO + NH₃ — i.e. the loss of the N- and C- termini leaving the side-chain intact. The m/z 126 peak has previously been identified as a novel marker ion for acetylated lysine by Kim et al. [36]. At larger collision energies, a more significant population of m/z 84 ($[\mathrm{H}_{10}\mathrm{C_5}\mathrm{NI}]^+$) forms, which, as will be described below, can result from a secondary fragmentation of the m/z 126 decomposition product.

Our simulations find that the primary CID pathway for acetyl-lysine-H+ involves the loss of C(OH) $_2$ (or H $_2$ O + CO) from the C-terminus to yield m/z 143 ([H $_{15}$ C $_7$ N $_2$ O]+). This chemical transformation occurs via a proton migration from the protonated N-terminus to the C-terminus. While the majority of the time this is a direct transfer, it is also possible for multiple proton hops to occur, with the acetyl's oxygen acting an intermediate protonation site. In either case, the most common final structure is protonated N-(5-iminopentyl) acetamide, making up 71.4% of the peak. Variations on this structure are seen in which a proton and/or the double bond has migrated, but all structures are straight-chain and maintain the same heavy atom sigma bonding framework, as shown in Fig. 2. All other peaks within the simulation are minor pathways; hence, we conclude that side-chain loss has been largely deactivated within the simulations' timescale.

Within the initial set of trajectories, the primary experimental peak $(m/z\ 126)$ was observed as a rare event in which $m/z\ 143$ was identified as an intermediate. To obtain a larger sample size of $m/z\ 126$ within simulations, two additional sets of calculations were performed: (1) 100 ps simulations of acetyl-lysine-H⁺ and (2) simulations starting from the most common structure within the $m/z\ 143$ peak with a 100 ps simulation and an internal energy of 250 kcal/mol. While both

Fig. 2. In simulations, the most commonly occurring structure in the m/z 143 peak is protonated N-(5-iminopentyl) acetamide at 71.4%. Several other structures in which a proton/double bond has migrated are also shown.

approaches did result in larger m/z 126 populations, it was determined that the second approach would enable obtaining a sufficient sample of post m/z 143 reactivity with less computational expense.

It was found that m/z 143 primarily decomposes into m/z 126, 101 $([H_{13}C_5N_2]^+)$, 84, 56 $([H_6C_3N]^+)$, and 43 $([CH_3CO]^+)$. The order of frequency of these secondary decomposition products is m/z 101, 84, 43, 126, and 56, respectively. As described above, m/z 126 and 84 are seen experimentally. Starting from acetyl-lysine-H+, the m/z 126 peak is formed via loss from both the N- and C- termini, namely loss of $NH_3 + C(OH)_2/H_2O + CO$. In our simulations, this most commonly occurs via a ring closure mechanism that is similar to pathway 4c of our previous work on lysine-H⁺ [14]. The m/z 84 peak forms through two different primary means: (1) directly from m/z 143 via the neutral loss of acetamide, and (2) indirectly via the subsequent loss from m/z 126 of the acetylation PTM as neutral ketene (CH2CO). These mechanisms are shown in Fig. 3. In our simulations, the direct loss pathway occurs \sim 40% of the time. In each case, the most common charged structure is N-protonated 1-Piperideine, which makes up a 59% of the peak with an additional 29% of the peak composed of straight-chain structures that could interconvert to N-protonated 1-Piperideine given sufficient time and energy. The remaining structures are likely transient intermediates that are captured at the end of the simulation time window.

The m/z 101 and 43 peaks are also closely related to these primary decomposition products with m/z 101 corresponding to the loss of ketene (CH₂CO) from m/z 143, while m/z 43 is protonated ketene ([CH₃CO]⁺). The former is likely a transient intermediate that will ultimately result in m/z 84, while the later could either transfer a proton back resulting in m/z 101 or could be the final product. The m/z 56 peak is the least commonly observed and forms following a hydrogen abstraction by the side-chain nitrogen from N-terminus from the β carbon of the side-chain to produce protonated aminoallene. Experimentally, our instrument cannot observe either m/z 43 or 56.

Fig. 3. The subsequent and direct mechanisms observed in simulations for the formation of the primary structure of m/z 84 from m/z 143.

3.3. Reactive pathways for TMe-lysine+

Compared to acetyl-lysine-H⁺, the decomposition chemistry in TMelysine⁺ is more straightforward and initiated by reactivity at the side-chain. The primary CID loss pathway involves population moving from m/z 189 ([H₂₁C₉N₂O₂]⁺) $\rightarrow m/z$ 130 ([H₁₂C₆NO₂]⁺) $\rightarrow m/z$

84 ([H₁₀C₅N]⁺), which corresponds to the initial loss of the sidechain followed by loss of $C(OH)_2$ or $H_2O + CO$ from the C-terminus. In contrast to acetyl-lysine-H+, the trimethylation of lysine has not deactivated the side-chain as the initial reactive site. The formation of trimethylamine is observed as a byproduct for both the m/z 130 and 84 peaks. Previous experimental work by Hirota et al. [37] also noted the formation of trimethylamine during the CID of TMe-lysine⁺. In addition, our simulations find that the formation of protonated trimethyl amine is now possible and corresponds to m/z 60. However, at the internal energies considered here it has a lower population than m/z 130 and 84. The formation of m/z 130 primarily results in the same structure observed in Pathway 1 of our previous work on lysine [14], and the most common m/z 84 structures also agree with that work. Although our simulations of TMe-lysine⁺ find that the most common m/z 84 product has a straight-chain structure, while those for acetyllysine-H⁺ find a cyclic structure, it is possible this is an artifact of the simulation time scale. Our previous DFT calculations [14] showed that the cyclic structure is more stable by ~94 kJ/mol. A minor pathway seen in the experiment that is absent in simulations is m/z 144, which corresponds to a mass loss of 42. Given that the loss of ketene was observed in the simulations of acetyl-lysine-H⁺, m/z 144 may be related to a direct ketene loss in this system.

4. Summary

Our experimental and computational results have highlighted the decomposition dynamics that are taking place in acetyl-lysine-H+ vs TMe-lysine+. Overall, acetyl-lysine-H+ is more reactive than TMelysine+, likely due to the latter's lack of an excess proton. While both species share several decomposition peaks in their CID spectra, they exhibit different mechanisms to reach these products. Reactivity at the side chain is reduced for acetyl-lysine-H+ lysine+, decomposition is often initiated at the PTM. The reactivity of TMe-lysine+is generally more straightforward while acetyl-lysineexhibits a more diverse set of reactive pathways. Simulations starting from acetyl-lysine-H⁺ largely yielded m/z 143. Pseudo MS3 simulations started with this decomposition product provided a sufficient population of subsequent decomposition products, including the experimentally observed m/z 126 and 84. We note that m/z 126 has previously been identified as a novel marker ion for acetylated lysine [36], and our simulations only show m/z 126 for acetyl-lysine-H⁺. The differences observed between the two systems again highlights that while the initial reactivity in acetyl-lysine-H+ is higher than TMe-lysine+, the subsequent decomposition dynamics, namely those involving the PTM, are hindered via acetylation.

At high energy - either collision energy in experiments, or internal energy in simulations - the primary decomposition product for both species is m/z 84. For TMe-lysine⁺, this product is formed via a mechanism similar to that seen in unmodified lysine [14], namely m/z 186 $\rightarrow m/z$ 130 $\rightarrow m/z$ 84. The acetylation PTM modifies this previously described mechanism by introducing m/z 143 as the new primary first step, with m/z 84 formed through two mechanisms: m/z $186 \rightarrow m/z$ $143 \rightarrow m/z$ $126 \rightarrow m/z$ 84 and m/z $186 \rightarrow m/z$ $143 \rightarrow m/z$ 84. Interestingly, while acetyl-lysine-H+ retains an excess proton, it is TMe-lysine⁺ that retains a similar mechanism to unmodified lysine. In both unmodified lysine and TMe-lysine+side-chain reactivity takes place through the loss of NH₃ or its methylated analog via a proton transfer from a carbon of the side-chain to the N-terminus. PTM of the side-chain does not impact this step, and hence the remainder of the mechanism can proceed. In contrast, acetylation results in a side-chain where this mechanism is hindered.

CRediT authorship contribution statement

George L. Barnes: Conceptualization, Software, Investigation, Writing. Kristopher J. Kolonko: Investigation, Writing. Kenneth Lucas: Investigation. Amy Chen: Investigation. Megan Schubmehl: Investigation.

Declaration of competing interest

The authors declare the following financial interests/personal relationships which may be considered as potential competing interests: George L. Barnes reports financial support was provided by National Science Foundation.

Data availability

Data will be made available on request.

Acknowledgments

The authors acknowledge the generous support from the National Science Foundation, United States under Grant No. 1763652 and 2301606. GLB is a member of the MERCURY consortium, which receives support through National Science Foundation, United States grant No. CHE-2018427.

References

- A. Kumar, V. Narayanan, A. Sekhar, Characterizing post-translational modifications and their effects on protein conformation using NMR spectroscopy, Biochemistry 59 (2020) 57–73, http://dx.doi.org/10.1021/acs.biochem.9b00827.
- [2] H. Ryšlavá, V. Doubnerová, D. Kavan, O. Vaněk, Effect of posttranslational modifications on enzyme function and assembly, J. Proteom. 92 (2013) 80–109, http://dx.doi.org/10.1016/j.jprot.2013.03.025.
- [3] C. Boscher, J.W. Dennis, I.R. Nabi, Glycosylation, galectins and cellular signaling, Curr. Opin. Cell Biol. 23 (4) (2011) 383–392, http://dx.doi.org/10.1016/j.ceb. 2011.05.001.
- [4] R.G. Cooks, T. Ast, T. Pradeep, V.H. Wysocki, Reactions of ions with organic surfaces, Acc. Chem. Res. 27 (11) (1994) 316–323, http://dx.doi.org/10.1021/ ar00047a001
- [5] I.A. Papayannopoulos, The interpretation of collision-induced dissociation tandem mass spectra of peptides, Mass Spectrom. Rev. 14 (1) (1995) 49–73, http://dx.doi.org/10.1002/mas.1280140104.
- [6] E.R. Williams, Tandem FTMS of large biomolecules, Anal. Chem. 70 (5) (1998) http://dx.doi.org/10.1021/ac981773x, arXiv:16532065, 179A-185A.
- [7] V.H. Wysocki, K.E. Joyce, C.M. Jones, R.L. Beardsley, Surface-induced dissociation of small molecules, peptides, and non-covalent protein complexes, J. Am. Soc. Mass Spectrom. 19 (2) (2008) 190–208, http://dx.doi.org/10.1016/j.jasms. 2007.11.005
- [8] A. Martin Somer, V. Macaluso, G.L. Barnes, L. Yang, S. Pratihar, K. Song, W.L. Hase, R. Spezia, Role of chemical dynamics simulations in mass spectrometry studies of collision-induced dissociation and collisions of biological ions with organic surfaces, J. Am. Soc. Mass Spectrom. 31 (1) (2020) 2–24, http://dx.doi.org/10.1021/jasms.9b00062.
- K. Lucas, G.L. Barnes, Modeling the effects of O-Sulfonation on the CID of Serine,
 J. Am. Soc. Mass Spectrom. 31 (5) (2020) 1114–1122, http://dx.doi.org/10. 1021/jasms.0c00037.
- [10] G.L. Barnes, A. Shlaferman, M. Strain, Fast fragmentation during surface-induced dissociation: An examination of peptide size and structure, Chem. Phys. Lett. 754 (2020) 137716, http://dx.doi.org/10.1016/j.cplett.2020.137716.
- [11] S. Pratihar, G.L. Barnes, W.L. Hase, S. Pratihara, G.L. Barnes, W.L. Hase, Chemical dynamics simulations of energy transfer, surface-induced dissociation, soft-landing, and reactive- landing in collisions of protonated peptide ions with organic surfaces, Chem. Soc. Rev. 45 (13) (2016) 3595–3608, http://dx.doi.org/ 10.1039/C5CS00482A.
- [12] S. Pratihar, G.L. Barnes, J. Laskin, W.L. Hase, Dynamics of protonated peptide ion collisions with organic surfaces, consonance of simulation and experiment, J. Phys. Chem. Lett. 7 (2016) 3142–3150, http://dx.doi.org/10.1021/acs.jpclett. 6b00978.
- [13] D. Frederickson, M. McDonough, G.L. Barnes, A computational comparison of soft landing of Alpha-Helical vs globular peptides, J. Phys. Chem. B 122 (41) (2018) 9549–9554, http://dx.doi.org/10.1021/acs.jpcb.8b06232.
- [14] K. Lucas, A. Chen, M. Schubmehl, K.J. Kolonko, G.L. Barnes, Exploring the effects of methylation on the CID of protonated lysine: A combined experimental and computational approach, J. Am. Soc. Mass Spectrom. 32 (2021) 2675–2684, http://dx.doi.org/10.1021/jasms.1c00225.
- [15] A.F. Perez-mellor, R. Spezia, Determination of kinetic properties in unimolecular dissociation of complex systems from graph-theory based analysis of an ensemble of reactive trajectories., J. Chem. Phys. 155 (12) (2021) 1–20, http://dx.doi.org/ 10.1063/5.0058382.

- [16] E. Martínez-Núñez, G.L. Barnes, D.R. Glowacki, S. Kopec, D. Peláez, A. Rodríguez, R. Rodríguez-Fernández, R.J. Shannon, J.J. Stewart, P.G. Tahoces, S.A. Vazquez, AutoMeKin2021: An open-source program for automated reaction discovery, J. Comput. Chem. 42 (28) (2021) 2036–2048, http://dx.doi.org/10.1002/jcc. 26734, arXiv:2105.03078.
- [17] S.A. Vázquez, X.L. Otero, E. Martinez-Nunez, A trajectory-based method to explore reaction mechanisms, Molecules 23 (12) (2018) 3156, http://dx.doi.org/ 10.3390/molecules23123156.
- [18] A. Rodríguez, R. Rodríguez-Fernández, S.A. Vázquez, G.L. Barnes, J.J.P. Stewart, E. Martínez-Núñez, Tsscds2018: A code for automated discovery of chemical reaction mechanisms and solving the kinetics, J. Comput. Chem. 39 (23) (2018) 1922–1930, http://dx.doi.org/10.1002/jcc.25370.
- [19] E. Rossich-Molina, J.-Y. Salpin, R. Spezia, E. Martinez-Nunez, On the gas phase fragmentation of protonated uracil: A statistical perspective, Phys. Chem. Chem. Phys. (2016) http://dx.doi.org/10.1039/C6CP01657J.
- [20] G.L. Barnes, W.L. Hase, Energy transfer, unfolding, and fragmentation dynamics in collisions of N-protonated octaglycine with an H-SAM surface, J. Am. Chem. Soc. 131 (47) (2009) 17185–17193, http://dx.doi.org/10.1021/ja904925p.
- [21] M.D. Hanwell, D.E. Curtis, D.C. Lonie, T. Vandermeersch, E. Zurek, G.R. Hutchison, Avogadro: An advanced semantic chemical editor, visualization, and analysis platform, J. Cheminform. 4 (1) (2012) 17, http://dx.doi.org/10.1186/1758-2946-4-17.
- [22] M.J. Abraham, T. Murtola, R. Schulz, S. Páll, J.C. Smith, B. Hess, E. Lindah, Gromacs: High performance molecular simulations through multi-level parallelism from laptops to supercomputers, SoftwareX 1–2 (2015) 19–25, http: //dx.doi.org/10.1016/j.softx.2015.06.001.
- [23] N. Schmid, A.P. Eichenberger, A. Choutko, S. Riniker, M. Winger, A.E. Mark, W.F. Van Gunsteren, Definition and testing of the GROMOS force-field versions 54A7 and 54B7, Eur. Biophys. J. 40 (7) (2011) 843–856, http://dx.doi.org/10. 1007/s00249-011-0700-9.
- [24] A.K. Malde, L. Zuo, M. Breeze, M. Stroet, D. Poger, P.C. Nair, C. Oostenbrink, A.E. Mark, An automated force field topology builder (ATB) and repository: Version 1.0, J. Chem. Theory Comput. 7 (12) (2011) 4026–4037, http://dx.doi.org/10.1021/ct200196m.
- [25] K.B. Koziara, M. Stroet, A.K. Malde, A.E. Mark, Testing and validation of the automated topology builder (ATB) version 2.0: Prediction of hydration free enthalpies, J. Comput. Aided Mol. Des. 28 (3) (2014) 221–233, http://dx.doi. org/10.1007/s10822-014-9713-7.
- [26] S. Canzar, M. El-Kebir, R. Pool, K. Elbassioni, A.E. Mark, D.P. Geerke, L. Stougie, G.W. Klau, Charge group partitioning in biomolecular simulation, J. Comput. Biol. 20 (3) (2013) 188–198, http://dx.doi.org/10.1089/cmb.2012.0239.
- [27] G.B. Rocha, R.O. Freire, A.M. Simas, J.J.P. Stewart, RM1: A reparameterization of AM1 for H, C, N, O, P, S, F, Cl, Br, and I, J. Comput. Chem. 27 (10) (2006) 1101–1111, http://dx.doi.org/10.1002/jcc.20425, arXiv:16691568.
- [28] J.P. Stewart, Mopac2016, 2016.
- [29] G.L. Barnes, K. Young, L. Yang, W.L. Hase, Fragmentation and reactivity in collisions of protonated diglycine with chemically modified perfluorinated alkylthiolate-self-assembled monolayer surfaces, J. Chem. Phys. 134 (9) (2011) 094106, http://dx.doi.org/10.1063/1.3558736.
- [30] Z. Homayoon, S. Pratihar, E. Dratz, R. Snider, R. Spezia, G.L. Barnes, V. Macaluso, A. Martin Somer, W.L. Hase, Model simulations of the thermal dissociation of the TIK(H⁺)₂ Tripeptide: Mechanisms and kinetic parameters, J. Phys. Chem. A 120 (42) (2016) 8211–8227, http://dx.doi.org/10.1021/acs.jpca.6b05884.
- [31] M. Gu, J. Zhang, W.L. Hase, L. Yang, Direct dynamics simulations of the thermal fragmentation of a protonated peptide containing arginine, ACS Omega 5 (3) (2020) 1463–1471, http://dx.doi.org/10.1021/acsomega.9b03091.
- [32] W.L. Hase, D.G. Buckowski, Monte carlo sampling of a microcanonical ensemble of classical harmonic oscillators, Chem. Phys. Lett. 74 (2) (1980) 284–287, http://dx.doi.org/10.1016/0009-2614(80)85159-1.
- [33] C. Schlier, A. Seiter, High-order symplectic integration: An assessment, Comput. Phys. Comm. 130 (1–2) (2000) 176–189, http://dx.doi.org/10.1016/S0010-4655(00)00011-4.
- [34] J.P. Stewart, Mopac2012, 2012.
- [35] Z. Gregg, W. Ijaz, S. Jannetti, G.L. Barnes, The role of proton transfer in surface-induced dissociation, J. Phys. Chem. C 118 (2014) 22149–22155, http://dx.doi.org/10.1021/jp507069x.
- [36] J.Y. Kim, K.W. Kim, H.J Kwon, D.W. Lee, Yoo. J.S., Probing lysine acetylation with a modification-specific marker ion using high-performance liquid chromatography/electrospray-mass spectrometry with collision-induced dissociation, 2002, http://dx.doi.org/10.1021/ac0256080, https://pubs.acs.org/doi/pdf/ 10.1021/ac0256080.
- [37] J. Hirota, Y. Satomi, K. Yoshikawa, T. Takao, ε-N, N, N-Trimethyllysine-specific ions in matrix-assisted laser desorption/ionization-tandem mass spectrometry, Rapid Commun. Mass Spectrom. 17 (5) (2003) 371–376, http://dx.doi.org/10. 1002/rcm.924.